Copyright Warning & Restrictions

The copyright law of the United States (Title 17, United States Code) governs the making of photocopies or other reproductions of copyrighted material.

Under certain conditions specified in the law, libraries and archives are authorized to furnish a photocopy or other reproduction. One of these specified conditions is that the photocopy or reproduction is not to be "used for any purpose other than private study, scholarship, or research." If a, user makes a request for, or later uses, a photocopy or reproduction for purposes in excess of "fair use" that user may be liable for copyright infringement,

This institution reserves the right to refuse to accept a copying order if, in its judgment, fulfillment of the order would involve violation of copyright law.

Please Note: The author retains the copyright while the New Jersey Institute of Technology reserves the right to distribute this thesis or dissertation

Printing note: If you do not wish to print this page, then select "Pages from: first page # to: last page #" on the print dialog screen

ABSTRACT

THE USE OF ELECTRICAL RESISTANCE TOMOGRAPHY TO DETERMINE THE MINIMUM AGITATION SPEED FOR SOLIDS SUSPENSION IN STIRRED TANK REACTORS

by

Baran Teoman

N_{js}, the minimum agitation speed needed to just suspend all the solid particles in a solid-liquid mixture stirred in an agitated vessel, is a critical parameter to properly operate industrial tanks in a large number of industrial operations. As a result, a significant literature on N_{js} is available. The oldest and the most common method to measure N_{js} experimentally is that of Zwietering's (*Chem. Eng. Sci.,* 1958, 8, 244-253), where N_{js} can be visually obtained by determining when the solids stay at the bottom of the tank for no more than 1-2 seconds before being swept away. Although this has been shown to be a reliable method, it still relies on visual observation of the bottom of the vessel and it is therefore potentially susceptible to observer's bias. To address this issue new experimental approaches to determine N_{js} using measurements of the fraction of solids on the vessel bottom were previously developed by our research group. However even those methods are unsuitable to be used in opaque fluids or if images of the vessel bottom cannot be taken.

In order to experimentally determine N_{js} even in systems where the tank content cannot be inspected, in this work a novel method using Electrical Resistance Tomography (ERT) was developed and tested. Accordingly, a sensor array probe consisting of a straight plastic rod mounting 16 electrodes was placed vertically in a tank containing water and non-conductive glass beads approximately 300 μm in diameter. The electrodes were connected to an external

ERT system and data acquisition apparatus (P2+ System, Industrial Tomography Systems, Manchester, UK) dynamically measuring the conductivity distribution and resistivity in the solid-liquid system data between the electrodes. The apparatus consisted of a signal source, voltmeters, electrode multiplexer array, signal demodulators, and a system controller, connected to a computer where image reconstruction algorithms generated 2-D images of the conductivity distribution inside the tank. The system generated Alternating Current (AC) between pairs of neighboring electrodes and the resulting voltage was measured across all other neighboring electrodes. Current injection was applied to all neighboring electrodes. Through this approach it was possible to measure the mean bulk resistance across the electrodes on the sensing array probe and also measure the conductivity distribution on a portion of a vertical place inside the tank.

Here the array probe was placed in the tank, and after proper calibration, the mean bulk resistance of the solid-liquid mixture was obtained as the mixture was stirred by an impeller in the mixing tank at different values of the impeller agitation speed, *N*. As *N* increased, increasing larger fractions of the non-conducting solids became suspended, thus increasing the resistivity of the suspension measured by the ERT apparatus. A plot of the percent resistance variation vs. the agitation speed resulted in an *S*-shaped curve, which eventually reached an asymptotic limit value as all solids became suspended and dispersed in the liquid. In order to extract N_{js} from the data, a mathematical approach previously developed by our groups for a different system was used (Huang and Armenante, *Chem. Eng. Sci.*, 1992, 47, 2865-2870). Accordingly, the experimental data were interpolated with cubic spline curves and the agitation speed at which the function $\Phi(N)$, equal to the ratio of the second derivative to the first derivative of

the combined spline curve function, showed a minimum point was takes as the N_{js} value ($N_{js\text{-}ERT}$). The rationale for this approach is as follows: Φ(N) represents how the change in slope of the spline curve (second derivative) with respect to the spline curve slope (first derivative) varies with N. Φ(N) can be expected to reach a minimum value when the spline function is just about to bend to approach the asymptote.

Experiments were conducted where N_{js} was obtained under different operating conditions, i.e., where the impeller type, impeller ratio-to-tank diameter ratio, and impeller clearance were varied. N_{js} was not only experimentally obtained using the proposed ERT approach but also using the Zwietering method as well as the method recently developed by Shastry and Armenante (Shastry, 2016). Then, parity plots were constructed in which $N_{js\text{-}ERT}$ was plotted against the N_{js} values obtained with the other two methods. Excellent agreement was observed in all plots, indicating that the novel method proposed here can be effectively used for the experimental determination of N_{js}.

The results of this work show that ERT combined with the analysis of the data proposed here can be used to effectively measure N_{js} in solid-liquid dispersion in mechanically stirred vessels. The proposed approach is observer-independent method and can be used even in systems that cannot be directly observed, such as industrial tanks. Therefore, it is expected that this approach could find extensive practical applications in the chemical, pharmaceutical and biopharmaceutical industries.

THE USE OF ELECTRICAL RESISTANCE TOMOGRAPHY TO DETERMINE THE MINIMUM AGITATION SPEED FOR SOLIDS SUSPENSION IN STIRRED TANK REACTORS

by
Baran Teoman

A Thesis
Submitted to the Faculty of
New Jersey Institute of Technology in Partial Fulfillment of the Requirements for the Degree of Master of Science in Pharmaceutical Engineering

Otto H. York Department of Chemical and Materials Engineering

May 2019

APPROVAL PAGE

THE USE OF ELECTRICAL RESISTANCE TOMOGRAPHY FOR THE DETERMINATION OF THE MINIMUM AGITATION SPEED FOR SOLIDS SUSPENSION IN STIRRED TANK REACTORS

Baran Teoman

Dr. Piero M. Armenante, Thesis Advisor — Date
Distinguished Professor of Chemical and Materials Engineering, NJIT

Dr. Ecevit Bilgili — Date
Associate Professor of Chemical and Materials Engineering, NJIT

Dr. Murat Guvendiren — Date
Assistant Professor of Chemical and Materials Engineering, NJIT

Dr. Andrei Potanin — Date
Associate Director – Colgate-Palmolive Company

BIOGRAPHICAL SKETCH

Author: Baran Teoman

Degree: Master of Science

Date: May 2019

Undergraduate and Graduate Education:

- Master of Science in Pharmaceutical Engineering,
  New Jersey Institute of Technology, Newark, NJ

- Bachelor of Science in Chemical Engineering,
  Yeditepe University, Istanbul, Turkey

To My Family and Friends

ACKNOWLEDGMENT

I have taken efforts to complete this study. However, it would not have been possible without the kind support and help of many individuals and organizations. I would like to extend my sincere thanks to all of them.

I am highly indebted to Dr. Piero M. Armenante for his guidance and constant supervision, as well as for providing necessary information & support in completing the project. Also, I like to thank Dr. Ecevit Bilgili, Dr. Murat Guvendiren and Dr. Andrei Potanin for their continuous support and guidance throughout the course of this project work**.**

My deepest gratitude to my parents & members of my family for their kind co-operation and encouragement, which helped me in completion of this study.

TABLE OF CONTENTS

TABLE OF CONTENTS

(Continued)

LIST OF TABLES

LIST OF TABLES
(Continued)

Table **Page**

LIST OF FIGURES

LIST OF FIGURES

(Continued)

LIST OF FIGURES

(Continued)

Figure **Page**

NOMENCLATURE

D	Impeller diameter (cm)
T	Tank diameter (cm)
H	Liquid height (cm)
C	Off-bottom clearance (cm)
N	Rotational speed (rpm)
N_{js}	Just-suspension speed for solid suspension
$N_{js\text{-}Zwietering}$	Just-suspension speed obtained using Zwietering's method
$N_{js\text{-}ImageJ}$	Just-suspension speed obtained using ImageJ thresholding method
$N_{js\text{-}ERT}$	Just-suspension speed obtained using electrical resistance tomography technique
MBR	Mean bulk resistivity (Ω m)
Φ(N)	The change in slope of the spline curve with respect to the spline curve slope that varies with N

CHAPTER 1

INTRODUCTION

1.1 Background Information

A large number of industrial operations involve the use of tanks equipped with impellers to conduct processes such as reactions, precipitations, dissolutions, crystallizations, and many others in which finely divided solids are contacted with the liquid in the tank. In this type of systems suspending solids off the tank bottom and bringing them in contact with the surrounding liquid is often a key requirement to achieve process objectives. Down-pumping, mixed or axial impellers are typically used for the purpose of suspending solids, since radial impellers require substantially higher power to achieve suspension. Radial impellers are, however, still relevant in solid-liquid mixing since this impeller geometry is often found in mixing tanks irrespective of their specific use. This design it is efficient for gas-liquid dispersion, although many such systems also contain solids, as in fermentation systems or three-phase reactors, which must be suspended (Paul et al., 2004).

The degree of solid suspension in stirred vessels is generally classified into three levels: on-bottom motion, complete off-bottom suspension, and uniform suspension (Paul et al., 2004). For many applications, it is often important just to provide enough agitation to completely suspend the solids off the tank bottom. Below this off-bottom particle suspension state, the total solid-liquid interfacial surface area is not completely or efficiently utilized. Therefore, it is important to be able to determine the impeller agitation speed N_{js}, at which the just-suspended state is achieved by the particles (Armenante and Uehara-Nagamine 1998). As a result, a significant amount of work been conducted over the years on the experimental determination of N_{js} and on the establishment of equations

correlating N_{js} to a geometric and operational variables of relevance for solid-liquid systems. (Zwietering, 1958; Armenante et al, 1992)

1.2 Objectives

Before attempting to correlate N_{js} with other relevant variables it is critical to be able to experimentally obtain N_{js} simply and reliably. The typical method to measure experimentally N_{js} is that of Zwietering's (1958). Accordingly, N_{js} is obtained by visually inspecting the tank bottom and visually determining the impeller agitation speed at which the solids are observed to rest on the tank bottom for no more than 1-2 seconds before being swept away. This method has been shown to have a reproducibility of about ±5%. Although this method is quite reliable and has been used extensively, there is clearly the need to develop a method that is not observer-dependent. In addition, this approach cannot be used in systems, such as industrial tanks and reactors, in which the vessel content or tank bottom cannot be observed.

In a previous study conducted in the Mixing Laboratory at NJIT, Shriarjun Shastry developed a new experimental method to determine N_{js} (Shastry, 2016). Accordingly, images of the tank bottom were captured in .jpg format by a digital camera. Each image was processed with the appropriate software (Image J) to determine the area still covered by solids at that speed. Increasing the agitation speed increased the amount of solids being suspended, resulting in a decrease in the area covered by solids at the bottom of the tank. Plots of the area covered by the solids vs. the corresponding agitation speed resulted in a linear function, which, when extrapolated to A going to zero, yielded the expected value of N_{js}. The values so obtained for N_{js} were then compared to the N_{js} value determined

visually using Zwietering's method the two approaches gave very similar results, thus validating Shastry's approach.

Although Shastry's approach is observer-independent, it is still unusable unless the vessel bottom can be observed. Therefore, the objective of this study was to investigate a novel method based on the use of Electric Resistance Tomography (ERT) that is not only completely observer-independent but also applicable to opaque systems. The basic hypothesis was that by using ERT it should be possible to determine how the mean bulk resistivity changes as non-conductive solids become suspended in a conductive liquid when the agitation speed is increased. Then by properly analyzing the data a successful attempt was made to extract N_{js} from the data. The remainder of this document describes the experimental system used to achieve this objective and the results obtained to develop and validated a new method to obtain N_{js} experimentally using ERT.

CHAPTER 2

EXPERIMENTAL APPARATUS, MATERIALS, AND METHODS

2.1. Apparatus

2.1.1. Electrical Resistance Tomography (ERT) Apparatus

Electrical Resistance Tomography (ERT) provides the capability to measure the conductivity distribution and resistivity data in a liquid mixture inside a given processing unit, such as a stirred tank or reactor, delivering time-evolving, multi-dimensional information about the variation in uniformity of the liquid, which often enhances fundamental process understanding and improves the design and operation of the process equipment (Stanley and Bolton, 2008).

Figure 2.1 ITS P2+ ERT Tomography Apparatus, Also Showing The Rod Sensor with Electrodes In The Foreground.

The ERT system used in this work included a sensor system, a Data Acquisition System - DAS (hardware), and a PC with control and data processing software. Fig. 1 shows a P2+ERT system manufactured by Industrial Tomography Systems (ITS) Inc. In general, ERT sensors consist of multiple electrodes placed on a rigid mounting probe. The distance between the electrodes are equal and they are usually manufactured from gold, platinum, stainless steel, brass, or silver. They probe must have characteristics such as low cost, ease of installation, good conductivity and resistance (Sharifi, M., Young, B., 2013). In previous work in mixing systems, stirred vessel with different kinds of baffle arrangements and mixing characteristics have been used, ranging in size from laboratory vessel 15-40 cm in diameter (Miettinen et al., 2003; Simmons et al., 2009) to tanks at the industrial plant scale with diameter up to 150 cm (Stanley et al., 2002). Fig. 2.2 shows the possible electrode arrangements on sensor probes used in work in stirred tanks.

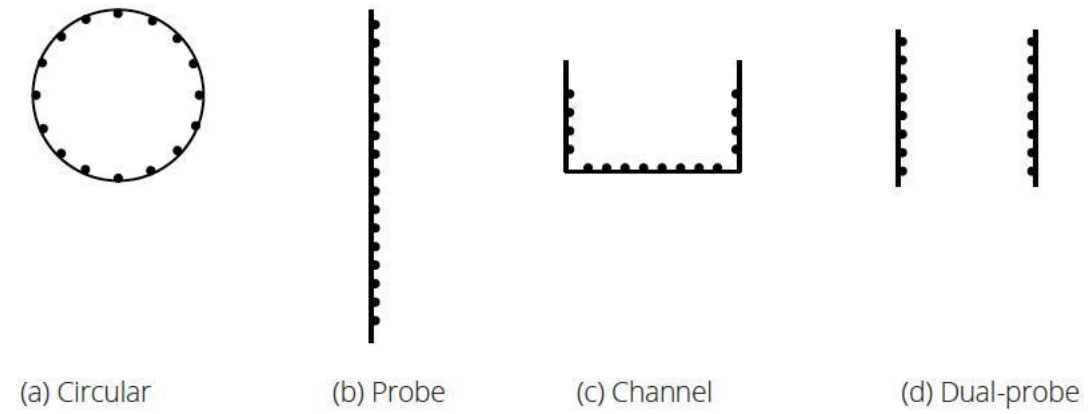

Figure 2.2 Schematic Representations of Sensor Geometries Showing The Electrode Arrangements on a Sensor Probe.

For radial profile studies in circular tanks, the circular electrode arrangement is common. However, in this work, since the main focus was on the axial profile distribution of solids in a liquid, a single straight-rod probe was used (Fig. 2 (b)). This probe, also shown in Fig. 1, consisted of a straight plastic rod mounting 16 electrodes connected via a cable to the main unit. The electrodes have 1 cm height and 2 cm width, and there was a 1 cm distance between each two following electrodes.

The data acquisition system (DAS) is the component of the system responsible with injecting electric current in the liquid in the tank via the electrode on probe and collecting quantitative information describing the conductivity distribution inside the vessel. DAS consists of signal sources, voltmeters, an electrode multiplexer array, signal demodulators, and a system controller. It has a connection with the probe and to the PC equipped the image reconstruction algorithms. In the adjacent strategy, which is the most common strategy in conventional ERT due to minimal hardware requirements and fast image reconstruction,

The DAS generates alternating current (AC) that is injected into the electrodes using a pair of neighboring electrodes. The resulting voltage is measured through all other neighboring electrodes. The current then goes to the next electrode pair and the process of injecting current to neighboring electrodes is repeated until all independent pairs have been covered (Mann et al., 1997).

2.1.2 Mixing Vessel and Impellers

A flat-bottomed cylindrical tank was used in all experimental work. The tank was placed on a glass board and raised to the required height using laboratory jacks. This set up can be seen in the Figure 2.3. The glass was transparent so that the tank bottom could be seen clearly in order to takes images of the same. The tank was provided with 4 baffles, 25 mm in width and thus was considered a fully baffled system. The mixing tank was filled with water so that the liquid level, H, was equal to 39 cm (H/T = 0.86), corresponding to a liquid volume, V, of 24 liters. Experiments in this system were conducted under variety of geometric configurations, including different impeller types, C/T and D/T.

Table 2.1 Geometric Characteristics of Mixing Tank

Tank Diameter (T)	28 cm
Tank Height	45 cm
Liquid Height (H)	39 cm
Tank Baffles	4
Tank Volume	29 L

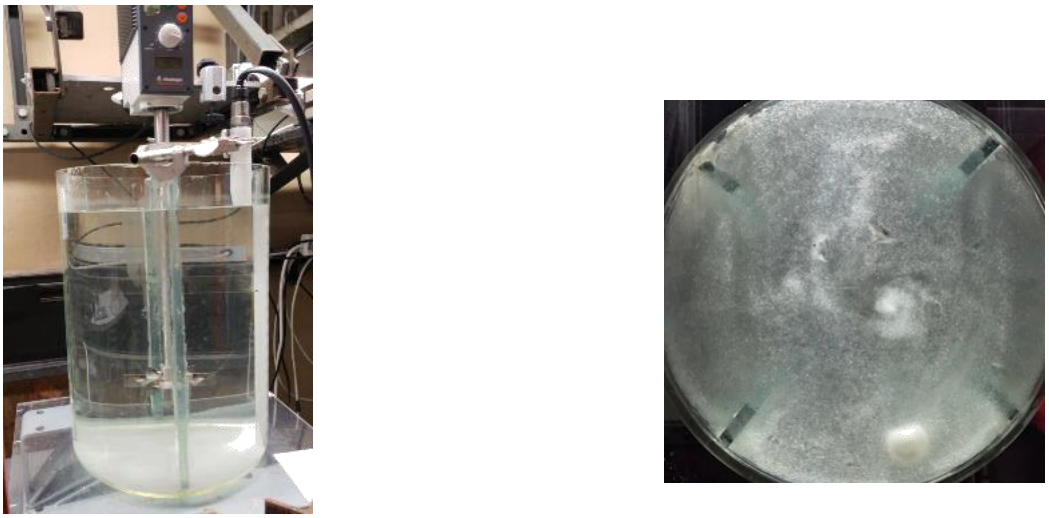

(a) (b)

Figure 2.3 (a) Flat-bottom Glass-lined Tank System; (b) Bottom View of The Tank Bottom with Dispersed Solids.

Five types of impellers, each type of different sizes. were used in this system, as shown in Figures 2.4 (a)-(e). These impellers which are scaled-down versions of impellers commonly used in the pharmaceutical industry and biopharmaceutical industry. The following are the impeller dimensions measured with a caliper:

Impeller 1: Disk Turbine

- impeller diameter (D) = 110 mm, 130 mm,
- blade height = 25.4 mm;
- blade thickness = 12.7 mm; and
- impeller diameter-to-tank diameter ratio, D/T, of 0.39, 0.46.

Impeller 2: Pitch Blade Turbine

- impeller diameter (D) = 110 mm, 80mm;

- blade height = 25.4 mm;
- blade thickness = 12.7 mm;
- impeller diameter-to-tank diameter ratio, D/T= 0.39 and 0.28.

Impeller 3: Flat blade turbine

- impeller diameter (D) = 100 mm;
- blade height = 25.4 mm;
- blade thickness = 12.7 mm; and
- impeller diameter-to-tank diameter ratio, D/T= 0.35.

Impeller 4: A310

- impeller diameter (D) = 100mm;
- blade height = 25.4 mm;
- blade thickness = 12.7 mm; and
- impeller diameter-to-tank diameter ratio, D/T=0.35.

Impeller 5: Propeller

- impeller diameter (D) = 100 mm;
- blade height = 25.4 mm;
- blade thickness = 12.7 mm; and
- impeller diameter-to-tank diameter ratio, D/T= 0.35.

(a)

(b)

(c)

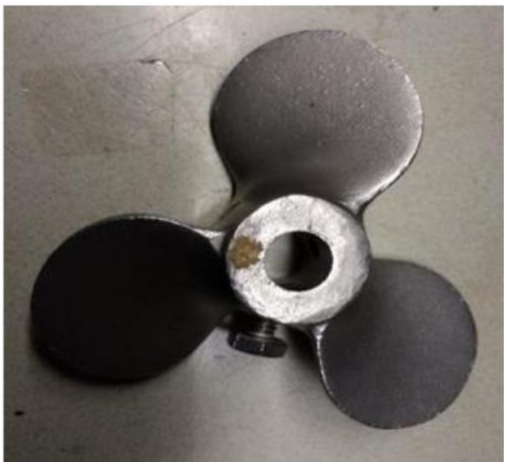

(d)

(e)

Figure 2.4 Impellers Used In This work: (a) A310; (b) FBT impeller; (c) 6-PBT; (d) Propeller; (e) DT

2.1.3. Agitation System

A Heidolph RZR 2102 agitator was used in the study because of its high agitation capabilities (12-2000 rpm). It is re-calibrated before each trial.

Figure 2.5 Agitation System

Table 2.2 Agitator Specifications

AC/DC input	**230 V**
feature	**CE compliant**
mfr. no.	**RZR 2102 Control**
measuring range	**100,000 viscosity, (mPas)**
parameter	**12-2000 rpm speed**
torque	**≤400 Ncm (peak overload)**
output	**100 watts**

2.2. Materials

Tap water at room temperature was used as the liquid in all experiments. The liquid height was equal to 39 cm in all cases. Glass beads having average of diameter of 300 μm were used as the disperse phase. In all of the experiments, the fraction of solids was equal to 0.2% of the liquid weight (g/g), corresponding to 52.3 g, as measured by an analytical balance.

2.3 Methods

In a typical experiment, the liquid and the solids were first added to the mixing tank. Then the appropriate impeller was mounted on the shaft, which was inserted in the agitation system, and the tank was centrally placed under the agitation system and positioned at a level so that the impeller had the desired vertical distance from the tank bottom, i.e., the desired off-bottom clearance (C). The agitations was started and the minimum agitation speed N_{js} at which all solids were just suspended was determined using the methods describe below.

2.3.1 Zwietering's Method to Determine N_{js}

The most common technique reported in the literature to measure the just-suspension speed is that of Zwietering's (Zwietering, 1958). Zwietering devised a simple visual technique in which the observer inspects the tank bottom, and visually determines the impeller agitation speed at which the solids stay on the tank bottom for no more than 1-2 seconds before being swept away. This agitation speed is considered as the just-suspension speed, N_{js}. Although this is a reliable method, it is clearly an observer-based and a novel method which does not depend on the observer would be preferred.

2.3.2 ImageJ Thresholding Method to Determine N_{js}

Another method to determine the just-suspension speed was developed previously in our laboratory. Digital photographic images of the tank bottom were obtained using a camera and sent to a computer in jpeg format for image analysis. By using ImageJ software (https://imagej.nih.gov/ij/), the images were converted to 8-bit images to quantitatively determine the area on the tank bottom covered by the solid particles at the time the image was taken. (Shastry, 2016) The internal diameter of the tank (28 cm) was used as a scale, as shown in Figure 2.7(a). A color threshold was set manually for the first image just to distinguish the black color portion of the image (corresponding to area occupied by solids) from the white areas (occupied by the water). With this approach the portion of the bottom covered by solids could be determined at any time and any agitation speed. This threshold was used for all other images to determine the area that is covered by the solids (A_s) at any agitation speed.

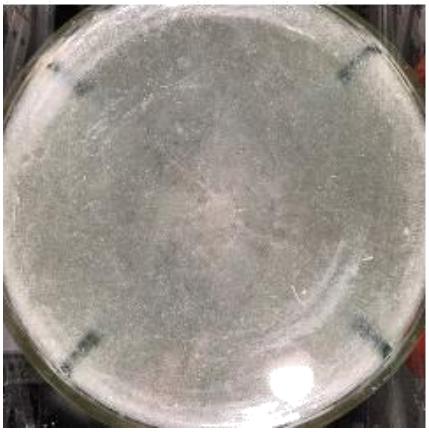

(a)

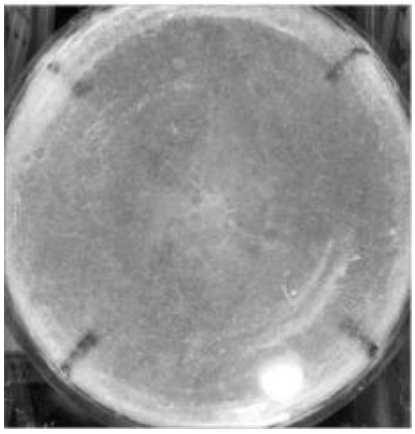

(b)

Figure 2.6 Images of Tank Bottom Analyzed Using ImageJ: (a) Raw Image of Tank Bottom (b) Conversion Into an 8-bit Image

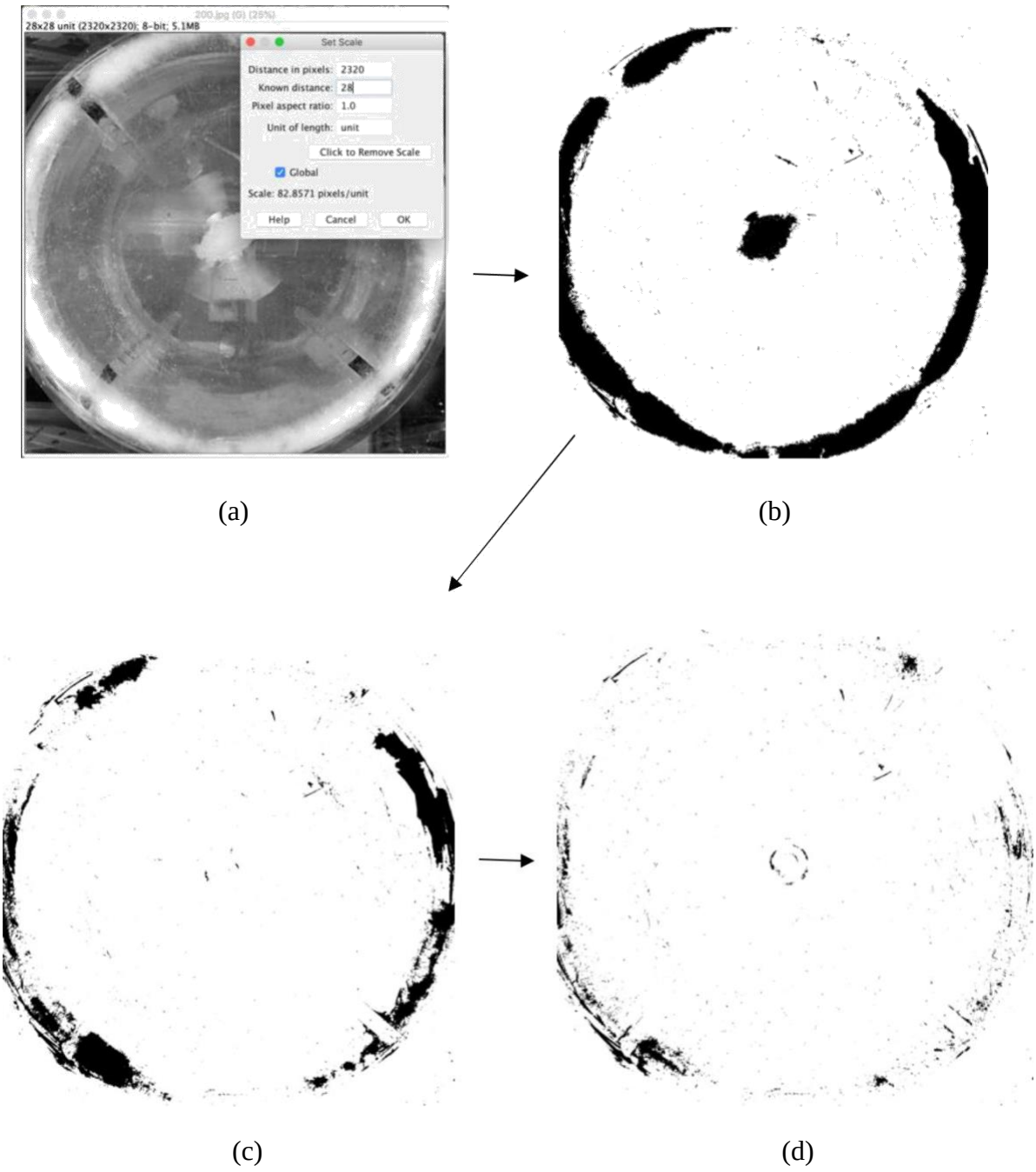

Figure 2.7 Images of Tank Bottom Analyzed Using ImageJ: (a) Raw Image and Scaling (b) Threshold at 200 rpm; (c) 300 rpm; (d) 350 rpm

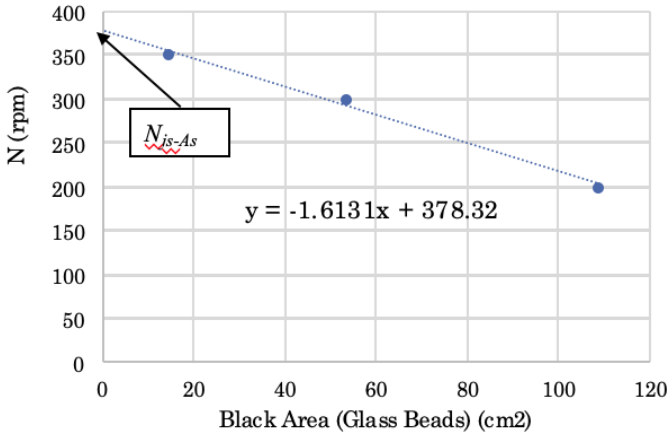

Figure 2.8 Agitation Speed vs. Area That Is Covered By Glass Beads

As the agitation speed was increased, the black area decreased as fewer solids remained on the tank bottom (although always moving). Plotting the agitation speed vs. the black area yields a linear trendline. The intercept of the equation of this trendline was taken as the just-suspension speed, N_{js}. This is because the intercept corresponds to agitation speed the black area vanishes and all the solids become suspended.

2.3.3 Tomography Method to Determine N_{js}

The third method, the main focus of this work, was the tomography method. By using the ITS P2+ electrical resistance tomography device, we speculated that the just-suspension speed can be related to the mean bulk resistivity data gathered from the tomography device. The tomography device consists of a linear probe, a data acquisition system and a software (ITS P2+). The linear sensor in the system contains 16 measurement electrodes and an earth electrode. The probe is made of glass, and the electrodes are made of embedded silver,

which provided a very good chemical compatibility. The bulk resistance data was used to estimate the just-suspension speed (N_{js}) because the definition of the bulk resistance relates to the mutual impedance as it is defined by the voltages measured across all electrodes by the injection current. (Ricard et al., 2005) Figure 2.9 illustrates the variation of the bulk resistance monitored as a function of PBT (Pitch Blade Turbine) impeller speed with C/T=0.25 for 0.2% solids loading.

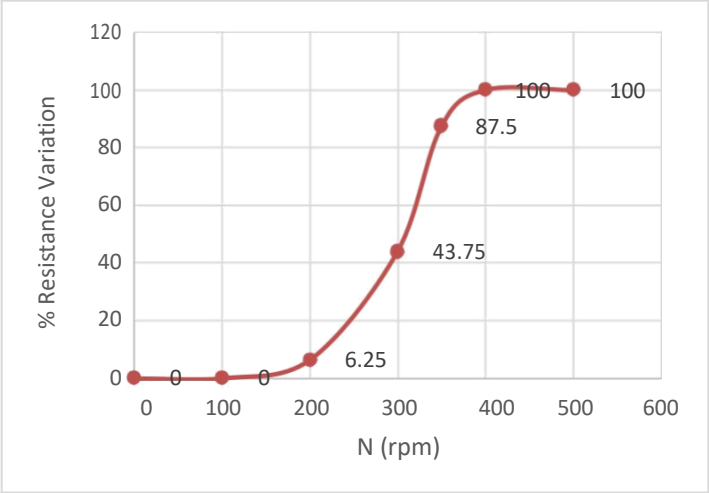

Figure 2.9 Variation of Average Bulk Resistance *R* with Agitation Speed *N* for a PBT (D/T=0.39, C/T = 0.25)

This figure shows that the % variation in the bulk resistance, R, of the vessel content increased as the agitation speed was increased, which is expected to be the case since as more non-conducting solid particles became suspended the average resistance of the mixture decreased until all solids are suspended, at which point the resistance no longer changed. More specifically, the S-shaped curve in this figure increased rapidly above an agitation speed of about 200 rpm (at very low agitation speeds all the solids are still on the bottom), and then passed through an inflexion point before becoming stable at a constant

value at very high impeller speeds. When the impeller was very close to the tank bottom (i.e. the clearance was very low) and axial impellers were used instead of radial impellers, or when the impeller blades were very close to the probe, a sudden increase in the resistance was observed just after the agitator was turned on. This led a double S-shaped plot of *R* vs. agitation speed. Figure 2.10 shows the variation of average bulk resistance with the agitation speed for propeller having the same clearance as the PBT impeller. The reason is that under these extreme low-C conditions, the impeller flow was mainly radial and directed outwards toward the tank wall which caused the immediate suspension of some centrally located particles at the vessel bottom. Thus, for best results, it was observed that the distance between the impeller blades and the probe should be no more than ¼ of the total length of the sensing probe. Nevertheless, even in those limit cases when the plot exhibited a double S-behavior, the determination of N_{js} was not affected since the just-suspension agitation condition is related to the asymptotic achievement of maximum resistance variation, i.e., to the last S-shaped curve.

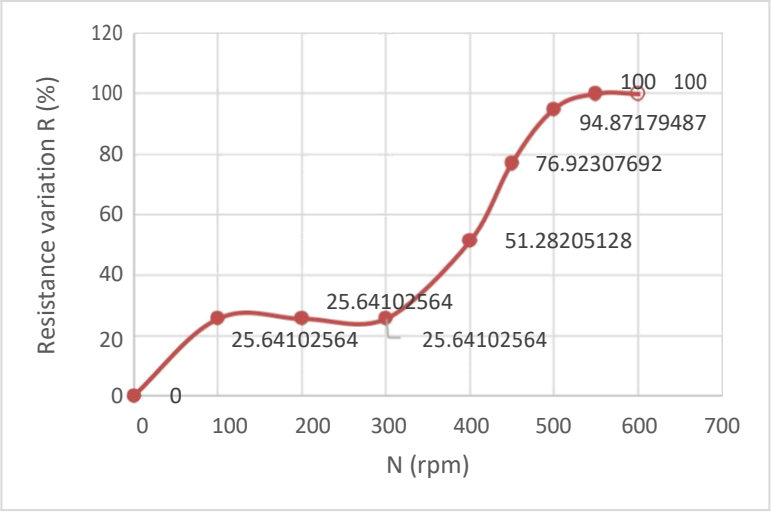

Figure 2.10 Variation of Average Bulk Resistance *R* with Agitation Speed *N* for a Propeller (D/T=0.35, C/T = 0.25).

The inflection point before the curve approached the asymptotic resistance value was related to the just-suspension speed, because when all the solids are suspended, the volume fractions of solids detected by the ERT sensor vary little. Here it was observed that that the achievement of approximately 99% of the variation in resistance corresponded to the attainment of the just-suspended conditions.

However, here a more mathematically rigorous approach was used here to obtain N_{js} from plots of % resistance variations vs. N. To do so, an approach similar to that used by Armenante and Abu-Hakmeh (Armenante and Abu-Hakmeh, 1994). These authors studied the agitation speed to achieve the just-dispersed state, N_{cd} in immiscible liquid-liquid mixtures. They collected samples from the same position inside the mixture and determined the fractions of the liquids in the samples at increasing agitation speeds. As the agitation speed increased, the mixture contained a larger fraction of the dispersed phase. They constructed a curve of dispersed phase vs. the agitation speed to determine at what speed the mixture reaches the just complete dispersion point. They then constructed a

cubic spline curve and they defined the function $\Phi(N)$, which represents the change in slope of the spline curve (second derivative) with respect to the spline curve slope (first derivative) varies with N. $\Phi(N)$ can be expected to reach a minimum value when the spline function is just about to bend to approach the asymptote.

A similar approach was used here using the tomography method for N_{js} instead of the sampling method for N_{cd}. To do so, a cubic spline curve was first constructed using the *R* vs. *N* data. This curve passed through all the *n* points on the graph and resulted in a composite set of cubic polynomial equations, with one polynomial equation connecting two adjacent points. This set of polynomial equations formed the entire spline curve. The

conditions imposed to determine the four coefficients in each cubic polynomial were the following:

- every polynomial must pass through exactly two points delimiting the interval for which the polynomial is being generated
- the first and second derivative of all polynomials must be identical at the points where they touch their adjacent polynomial.
- The second derivatives of the polynomial passing through initial point and of that passing through the final point must be equal to 0 (*"Natural Spline"*).

The determination for N_{js} from the spline curve R= $f(N)$ was conducted as follows. The function $\Phi(N)$ was defined as:

$$\Phi(N) = \frac{f''(N)}{f'(N)} \tag{1}$$

where $f'(N)$ and $f''(N)$ represent the first derivative and second derivative of $f(N)$, respectively. The ratio $f''(N)/f'(N)$ is the ratio of the rate of change of the slope of the curve, $f''(N)$, with respect to the slope itself, $f'(N)$. This ratio will be the greatest (in absolute value) when:

$$\Phi'(N) = 0 \tag{2}$$

The value of N in correspondence to which $\Phi'(N) = 0$ is taken to be the value of N_{js}. The reason for this is the following. Since the function $\Phi(N)$ represents the ratio of the rate of change in the slope of the curve $R = f(N)$ to the value of the slope of $f(N)$ it follows that $\Phi(N)$ can be assumed to be the highest (in absolute value) in correspondence of the minimum agitation speed for complete solid suspension. In fact, when this happens the rate at which

new solids can be expected to become suspended drop significantly. In addition, since the experimental values of R increase with N at a declining rate in the neighborhood of N_{js} the function $\Phi(N)$ must be negative in correspondence of this point. The experimental N_{js} value obtained with this approach was labeled $N_{js\text{-}ERT}$. In order to distinguish the value of N_{js} so obtained from those obtained using the Zwietering method and ImageJ method of Shastry and Armenante, these two N_{js} were labeled $N_{js\text{-}Zwietering}$ and $N_{js\text{-}ImageJ}$, respectively.

Just to provide an example, the critical points that are necessary for the determination of N_{js} with the PBT impeller (with C/T=0.25, and D/T=0.28) as described in Figure 2.9, are the resistivity values corresponding to the ones between 200-400 rpm. The reason is that until N=200 rpm, there is no significant change in the behavior of the curve. Since after 400 rpm there wasn't any change in the resistivity, the measurements at higher agitation speeds were not included because that would not have any effect on the curve.

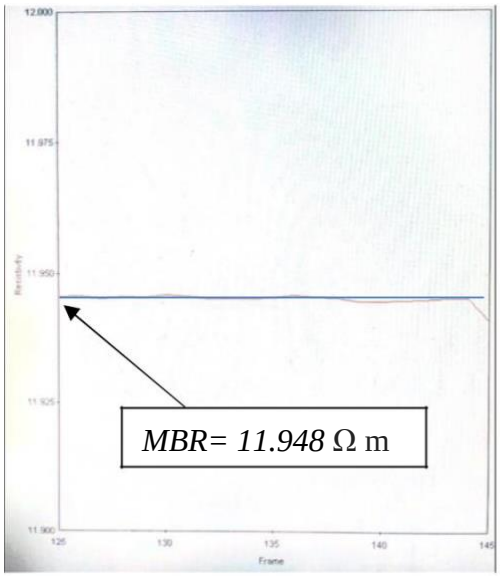

(a)

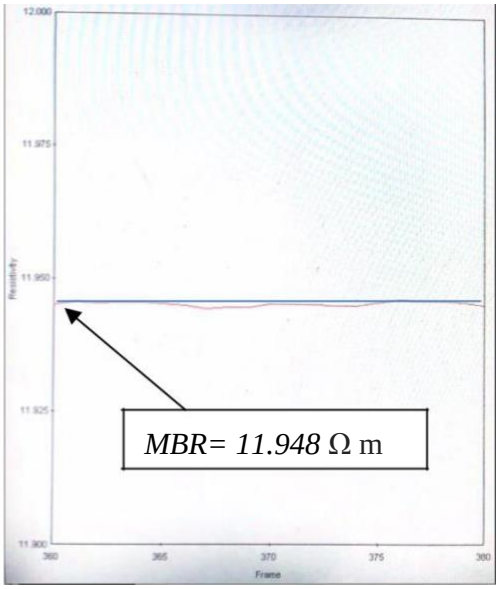

(b)

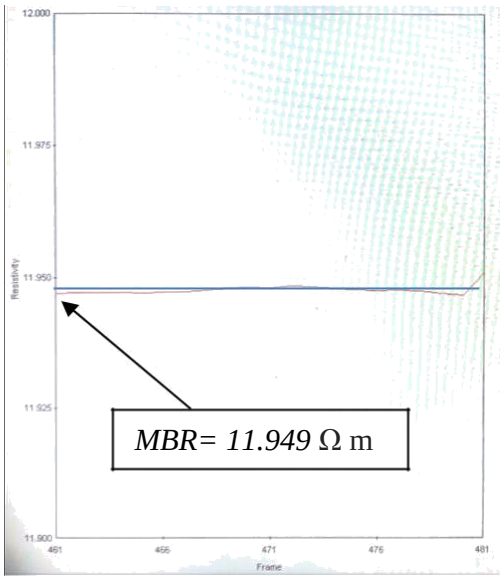

(c)

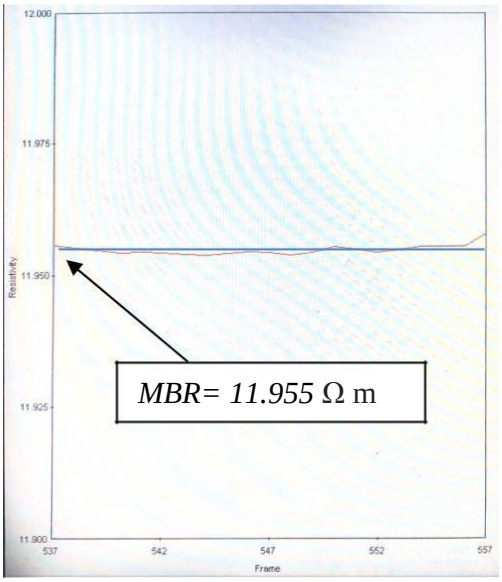

(d)

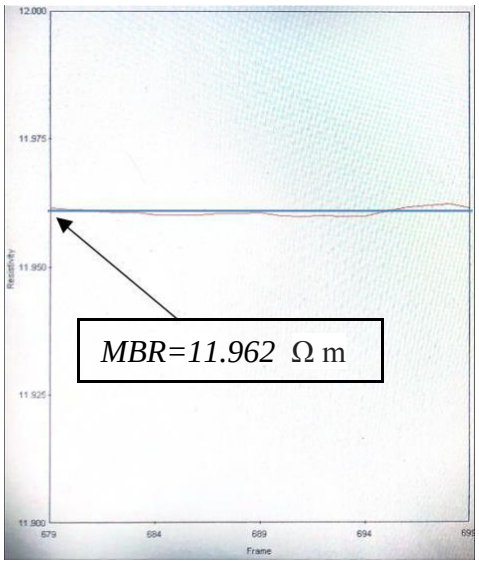

(e)

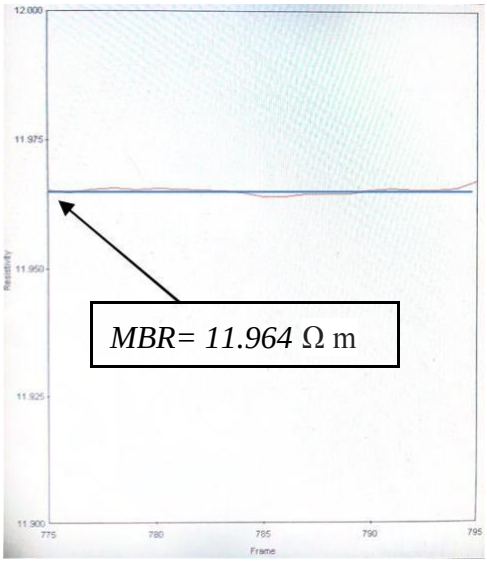

(f)

Figure 2.11 Mean Bulk Resistivity Lines Obtained From The ITS P2+ Software for PBT Impeller (with C/T=0.25, and D/T=0.28): (a) N=0 rpm, (b) N=100 rpm, (c) N=200 rpm, (d) N=300 rpm, (e) N=350 rpm, (f) N=400 rpm

Table 2.3 Mean Bulk Resistivity Output From The Tomography Device for a PBT (D/T=0.39, C/T = 0.25)

N (rpm)	Mean Bulk Resistivity (Ω·m)	Resistance Variation, R (%)
0	11.948	0
100	11.948	0
200	11.949	6.25
300	11.955	43.75
350	11.962	87.5
400	11.964	100
500	11.964	100

Figure 2.12 and 2.13 show the cubic spline curve and the interpolation output for the last 4 points of the data. An online cubic spline interpolator was used (https://tools.timodenk.com/cubic-spline-interpolation) for this manner. From the curve, it is clearly seen that N_{js} is somewhere between N=350 rpm and N=400 rpm as the curve became inflected in that interval.

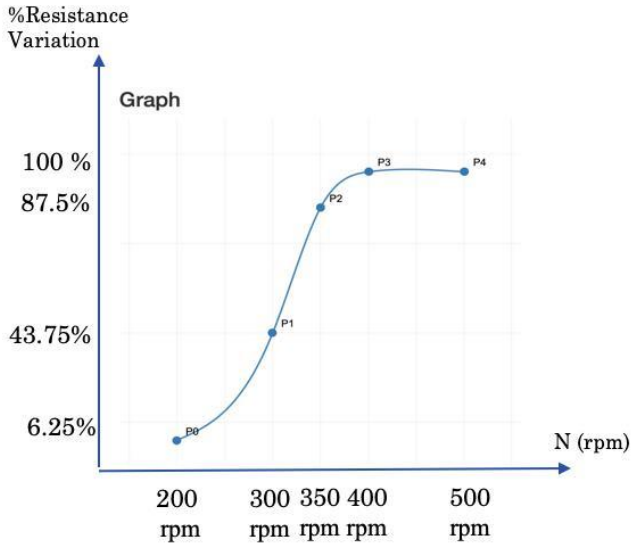

Figure 2.12 Cubic Spline Curve for Critical Points (Resistivity vs. N graph)

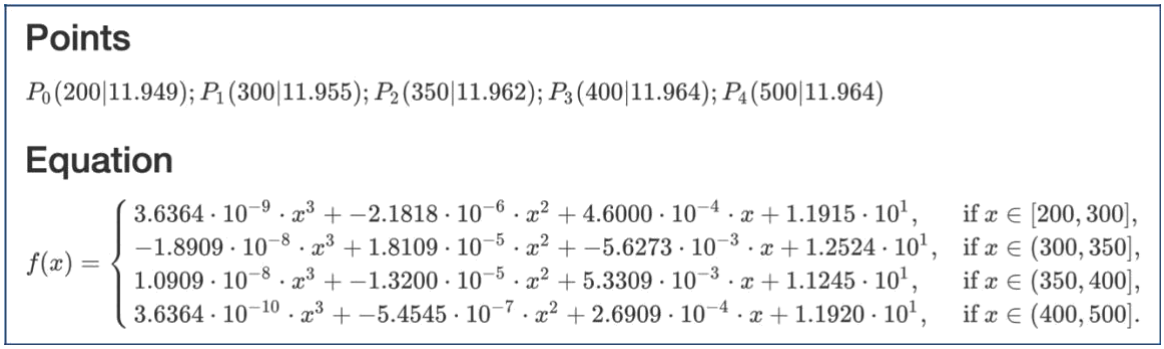

Figure 2.13 Cubic Spline Interpolation Output

Taking the first and second derivatives of the equation of the critical range (i.e. 350-400 rpm) yields:

$f(x) = 1.0909.10^{-8}.x^3 - 1.3200.10^{-5}.x^2 + 5.3309.10^{-3}.x + 1.1245.10^{1}$

$f'(x) = 3.2727.10^{-8}.x^2 – 2.6400.10^{-5}.x + 5.3309.10^{-3}$

$f''(x) = 6.5454.10^{-8}.x – 2.6400.10^{-5}$

Table 2.4 shows the derivative outputs for different agitation speeds. As it can be seen from the table, the ratio of the second derivative to the first derivative has the highest value (in absolute value) when N=388 rpm. As shown in Figure 2.14, at that point, $\Phi'(N)=0$ and it gives the just-suspension speed. Similarly, as shown in Figure 2.15, for propeller with C/T=0.25, and D/T=0.35, it was found that N=528 rpm was necessary for complete solid suspension.

Table 2.4 Derivative Table for PBT Impeller (with C/T=0.25, and D/T=0.28)

x = RPM	F'(x)	F"(x)	F"(x)/F'(x)
350	9.99575E-05	-3.4911E-06	-0.0349258
352	9.31062E-05	-3.36019E-06	-0.0360899
354	8.65167E-05	-3.22928E-06	-0.0373255
356	8.01891E-05	-3.09838E-06	-0.0386384
358	7.41232E-05	-2.96747E-06	-0.0400343
360	6.83192E-05	-2.83656E-06	-0.0415192
362	6.2777E-05	-2.70565E-06	-0.0430994
364	5.74966E-05	-2.57474E-06	-0.0447808
366	5.2478E-05	-2.44384E-06	-0.0465688
368	4.77212E-05	-2.31293E-06	-0.0484675
370	4.32263E-05	-2.18202E-06	-0.050479
372	3.89932E-05	-2.05111E-06	-0.0526018
374	3.50219E-05	-1.9202E-06	-0.0548287
376	3.13124E-05	-1.7893E-06	-0.0571435
378	2.78647E-05	-1.65839E-06	-0.0595158
380	2.46788E-05	-1.52748E-06	-0.0618944
382	2.17547E-05	-1.39657E-06	-0.0641962
384	1.90925E-05	-1.26566E-06	-0.0662911
386	1.66921E-05	-1.13476E-06	-0.0679817
388	1.45535E-05	-1.00385E-06	-0.0689765
390	1.26767E-05	-8.7294E-07	-0.0688618
392	1.10617E-05	-7.42032E-07	-0.067081
394	9.70857E-06	-6.11124E-07	-0.0629468
396	8.61723E-06	-4.80216E-07	-0.0557274
398	7.78771E-06	-3.49308E-07	-0.0448538
400	0.00000722	-2.184E-07	-0.0302493

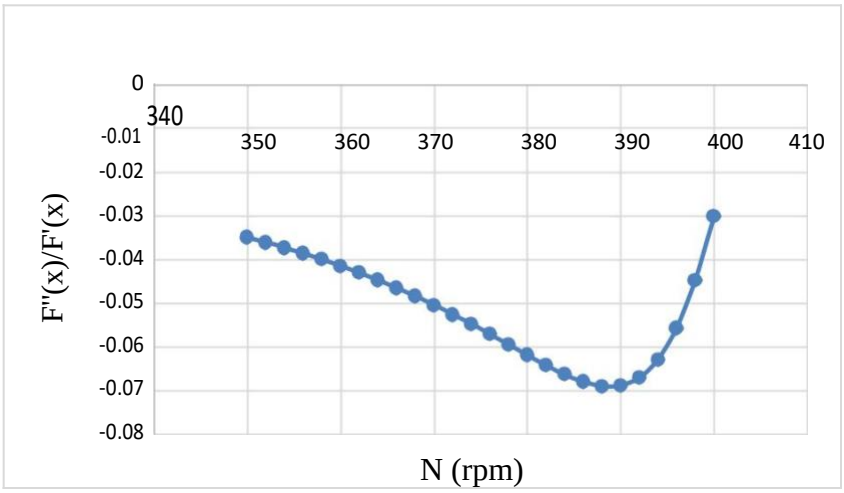

Figure 2.14 F'(x)/F(x) vs N Graph for PBT Impeller (with C/T=0.25, and D/T=0.39)

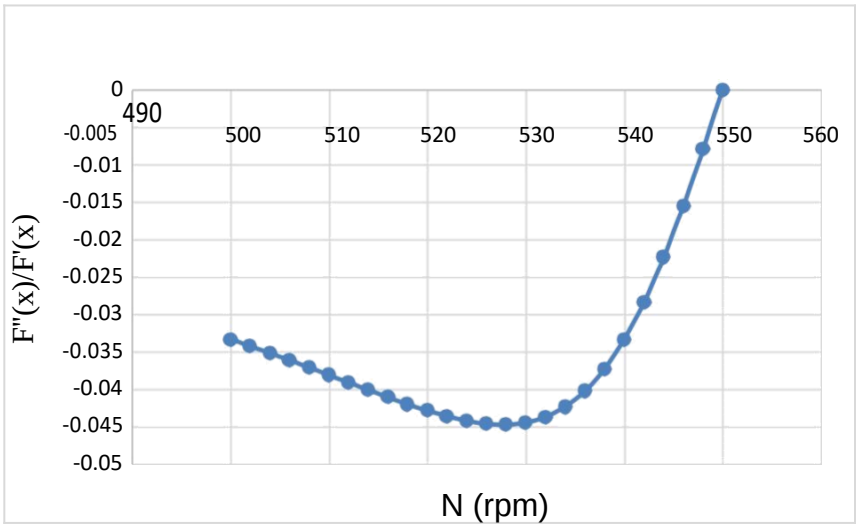

Figure 2.15 F'(x)/F(x) vs N Graph for Propeller (with C/T=0.25, and D/T=0.35)

After the determination of the N_{js} by using the described method, the $N_{js\text{-ERT}}$ value is compared to the ones that were obtained from the first two methods (Zwietering and ImageJ methods).

Table 2.5 Derivative Table For Propeller (with C/T=0.25, and D/T=0.35)

RPM	F'(x)	F"(x)	F"(x)/F'(x)
500	0.00009	-0.000003	-0.033333333
502	0.00008412	-0.00000288	-0.034236805
504	0.00007848	-0.00000276	-0.035168196
506	0.00007308	-0.00000264	-0.036124795
508	0.00006792	-0.00000252	-0.037102473
510	0.000063	-0.0000024	-0.038095238
512	0.00005832	-0.00000228	-0.03909465
514	0.00005388	-0.00000216	-0.040089087
516	0.00004968	-0.00000204	-0.041062802
518	0.00004572	-0.00000192	-0.041994751
520	0.000042	-0.0000018	-0.042857143
522	0.00003852	-0.00000168	-0.043613707
524	0.00003528	-0.00000156	-0.044217687
526	0.00003228	-0.00000144	-0.044609665
528	**0.00002952**	**-0.00000132**	**-0.044715447**
530	0.000027	-0.0000012	-0.044444444
532	0.00002472	-0.00000108	-0.04368932
534	0.00002268	-0.00000096	-0.042328042
536	0.00002088	-0.00000084	-0.040229885
538	0.00001932	-0.00000072	-0.037267081
540	0.000018	-0.0000006	-0.033333333
542	0.00001692	-0.00000048	-0.028368794
544	0.00001608	-0.00000036	-0.02238806
546	0.00001548	-0.00000024	-0.015503876
548	0.00001512	-0.00000012	-0.007936508
550	0.000015	0	0

CHAPTER 3

RESULTS AND DISCUSSION

3.1 Results of Solid Suspension Experiments

In this section, the results of the experiments are presented and compared to the ones that were obtained with using Zwietering's method and ImageJ method. Furthermore, reproducibility of the proposed method was also quantified.

Using to the approach developed here to obtain N_{js} using the ERT method, mean bulk resistivity values were obtained from the tomography device at increasing values of the agitation speed, N. For every impeller, the experiment was repeated with different C/T (impeller off-bottom clearance). Different D/T values were also tested for PBT and DT impellers. Then, all the N_{js} results obtained with ERT method ($N_{js\text{-}ERT}$) were compared in parity plots with the N_{js} obtained using the other two methods ($N_{js\text{-}Zwietering}$ and $N_{js\text{-}ImageJ}$) for the same systems.

3.1.1 Results for A310 Impeller

Table 3.1 presents the results obtained with the A310 impeller and Figure 3.1 and Figure 3.2 parity plots in of $N_{js\text{-}ERT}$ vs. $N_{js\text{-}Zwietering}$ and $N_{js\text{-}ERT}$ vs. $N_{js\text{-}ImageJ}$, respectively. As one can see, there is significant agreement between the newly proposed ERT method and the other two methods. The typical difference between $N_{js\text{-}ERT}$ and the $N_{js\text{-}Zwietering}$ was 2.05% and that between $N_{js\text{-}ERT}$ and the $N_{js\text{-}ImageJ}$ was 2.39%.

Table 3.1 N_{js} Values Obtained From 3 Different Methods with Using A310 Impeller with Different C/T.

C/T	$N_{js\text{-}ERT}$ **(rpm)**	$N_{js\text{-}Zwietering}$ **(rpm)**	$N_{js\text{-}ImageJ}$ **(rpm)**
0.25	482	470	474
0.33	515	500	521
0.5	665	660	674

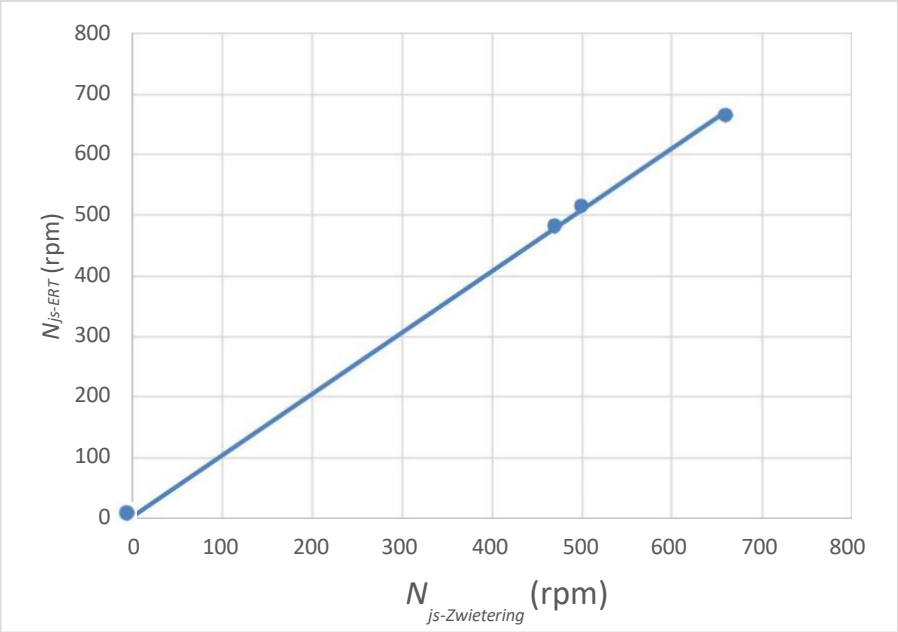

Figure 3.1 $N_{js\text{-}ERT}$ vs $N_{js\text{-}Zwietering}$ Comparison for A310 Impeller with D/T= 0.35 and with C/T=0.25, C/T=0.33, C/T= 0.5

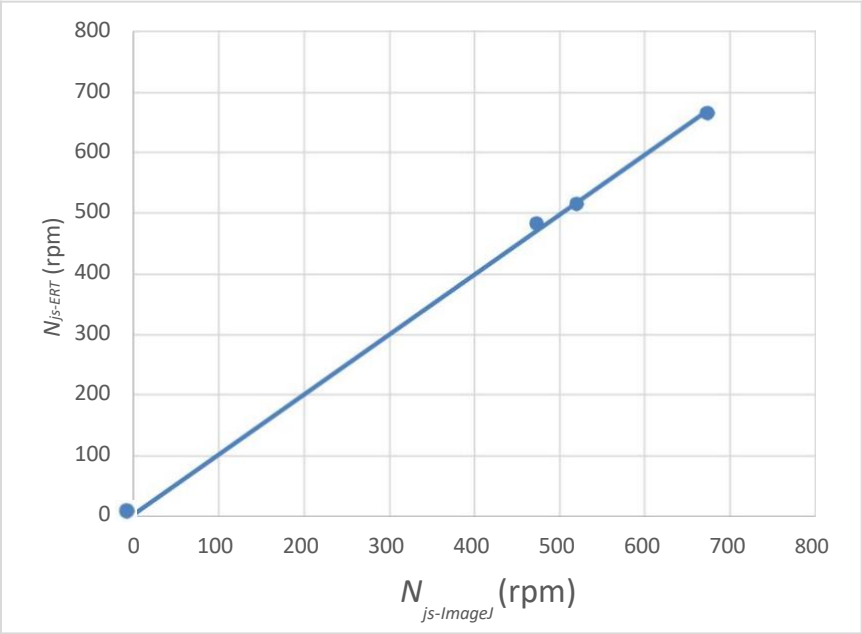

Figure 3.2 $N_{js\text{-}ERT}$ vs $N_{js\text{-}ImageJ}$ Comparison for A310 Impeller with D/T= 0.35 and with C/T=0.25, C/T=0.33, C/T= 0.5

3.1.2 Results for PBT Impeller

Table 3.2 presents the results obtained with the PBT impeller with D/T= 0.39 and Figure 3.3 and Figure 3.4 parity plots in of $N_{js\text{-}ERT}$ vs. $N_{js\text{-}Zwietering}$ and $N_{js\text{-}ERT}$ vs. $N_{js\text{-}ImageJ}$, respectively. Similarly, Table 3.3 presents the results with D/T=0.28 and Figure 3.5 and 3.6 parity plots in of $N_{js\text{-}ERT}$ vs. $N_{js\text{-}Zwietering}$ and $N_{js\text{-}ERT}$ vs. $N_{js\text{-}ImageJ}$, respectively. As one can see, there is significant agreement between the newly proposed ERT method and the other two methods. The typical difference between $N_{js\text{-}ERT}$ and the $N_{js\text{-}Zwietering}$ was 2.45% and that between $N_{js\text{-}ERT}$ and the $N_{js\text{-}ImageJ}$ was 2.38%.

Table 3.2 N_{js} Values Obtained from 3 Different Methods with Using PBT Impeller, D/T=0.39, with different C/T

C/T	$N_{js\text{-}ERT}$ **(rpm)**	$N_{js\text{-}Zwietering}$ **(rpm)**	$N_{js\text{-}ImageJ}$ **(rpm)**
0.25	388	365	378
0.33	530	515	512
0.4	655	675	668

Table 3.3 N_{js} Values Obtained from 3 Different Methods with Using PBT Impeller, D/T=0.28, with Different C/T

C/T	$N_{js\text{-}ERT}$ **(rpm)**	$N_{js\text{-}Zwietering}$ **(rpm)**	$N_{js\text{-}ImageJ}$ **(rpm)**
0.2	432	430	440
0.25	480	475	489
0.33	690	680	708

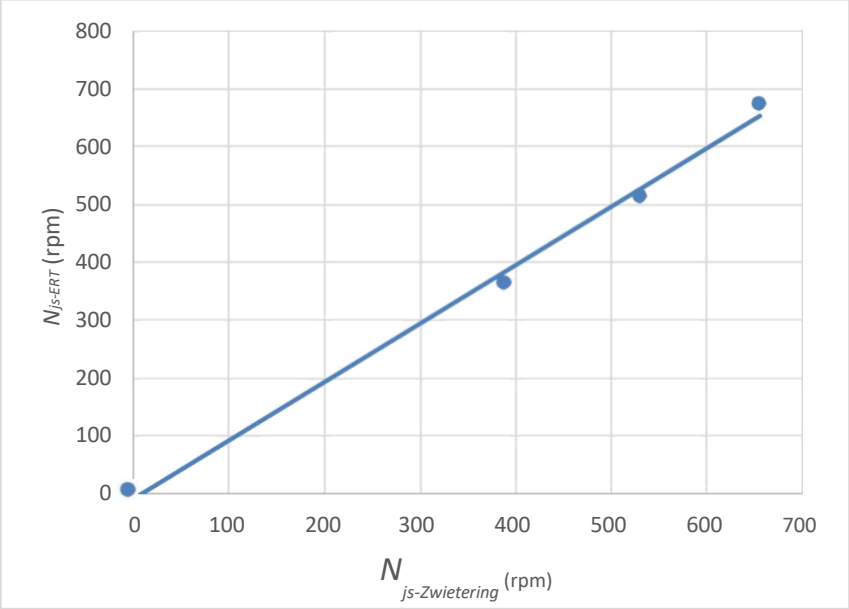

Figure 3.3 $N_{js\text{-}ERT}$ vs $N_{js\text{-}Zwietering}$ Comparison for PBT Impeller with D/T= 0.39 and with C/T=0.25, C/T=0.33, C/T= 0.5

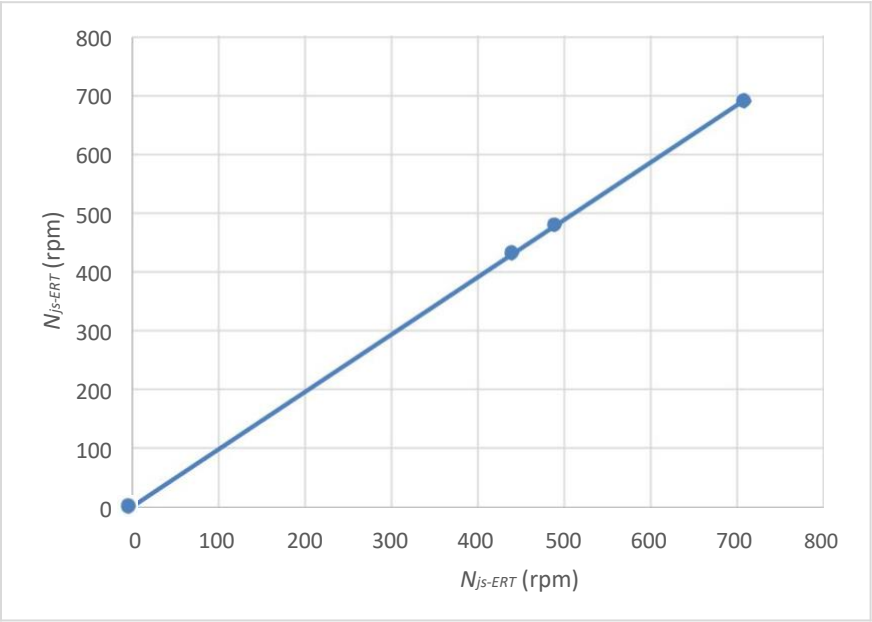

Figure 3.4 $N_{js\text{-}ERT}$ vs $N_{js\text{-}ImageJ}$ Comparison for PBT Impeller with D/T= 0.39 and with C/T=0.25, C/T=0.33, C/T= 0.5

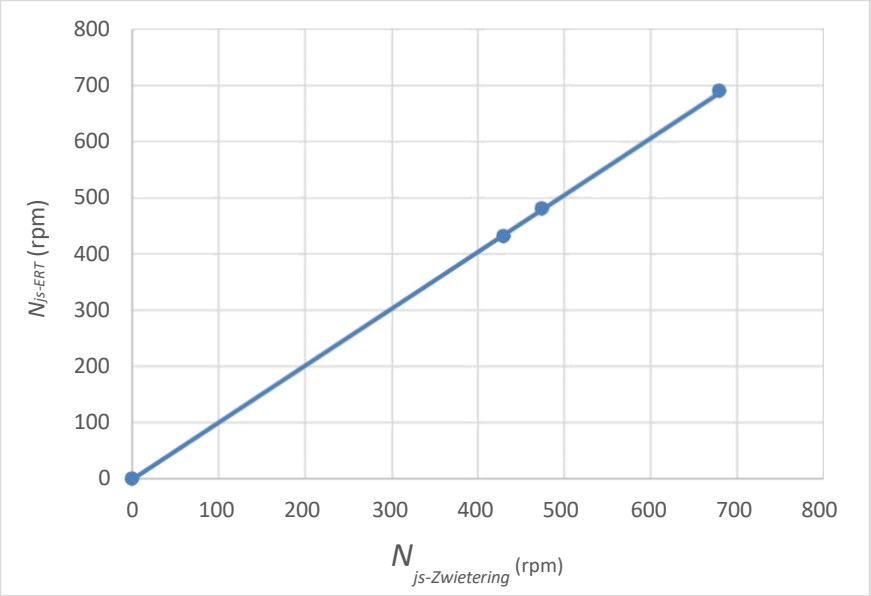

Figure 3.5 $N_{js\text{-}ERT}$ vs $N_{js\text{-}Zwietering}$ Comparison for PBT Impeller with D/T=0.28 and with C/T=0.2, C/T=0.25, C/T= 0.33

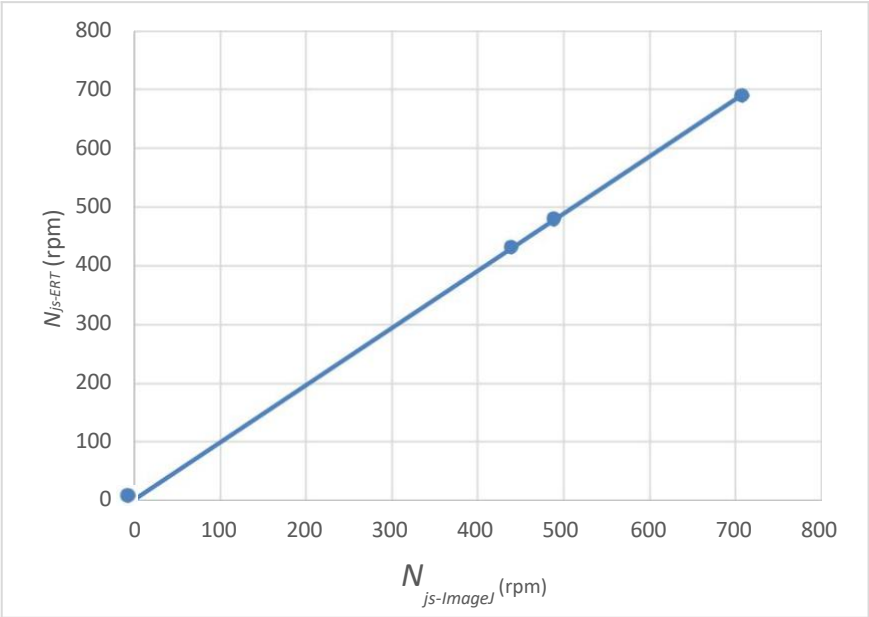

Figure 3.6 $N_{js\text{-}ERT}$ vs $N_{js\text{-}ImageJ}$ Comparison for PBT Impeller with D/T=0.28 and with C/T=0.2, C/T=0.25, C/T=0.33

3.1.3 Results for FBT Impeller

Table 3.4 presents the results obtained with the FBT impeller with D/T=0.35 and Figure 3.7 and Figure 3.8 parity plots in of $N_{js\text{-}ERT}$ vs. $N_{js\text{-}Zwietering}$ and $N_{js\text{-}ERT}$ vs. $N_{js\text{-}ImageJ}$, respectively. As one can see, there is significant agreement between the newly proposed ERT method and the other two methods. The typical difference between $N_{js\text{-}ERT}$ and the $N_{js\text{-}Zwietering}$ was 2.64% and that between $N_{js\text{-}ERT}$ and the $N_{js\text{-}ImageJ}$ was 1.61%.

Table 3.4 N_{js} Values Obtained from 3 Different Methods with Using FBT Impeller, D/T=0.28, with Different C/T

C/T	$N_{js\text{-}ERT}$ **(rpm)**	$N_{js\text{-}Zwietering}$ **(rpm)**	$N_{js\text{-}ImageJ}$ **(rpm)**
0.25	380	390	381
0.33	445	460	451
0.4	520	530	533

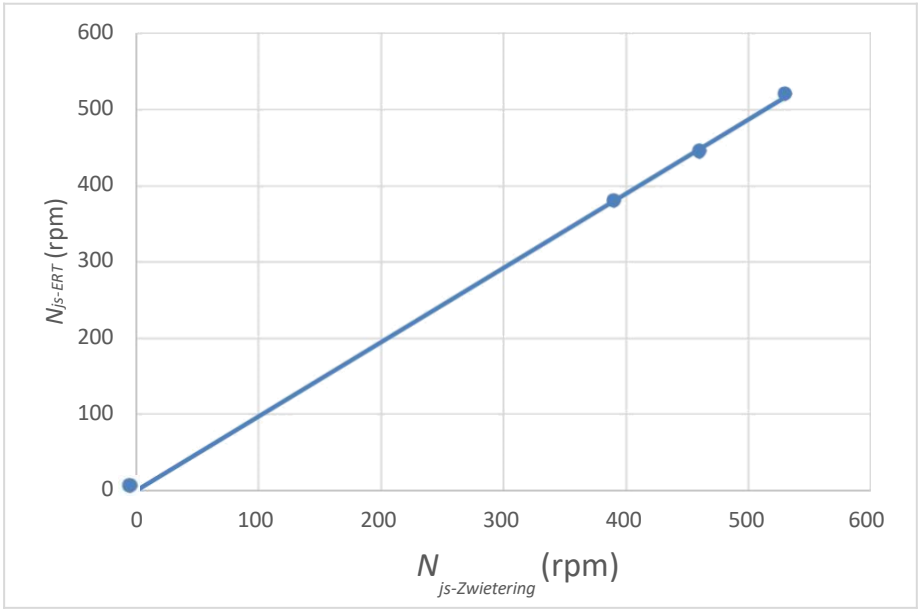

Figure 3.7 $N_{js\text{-}ERT}$ vs $N_{js\text{-}Zwietering}$ Comparison for FBT Impeller with D/T=0.35 and with C/T=0.25, C/T=0.33, C/T= 0.4

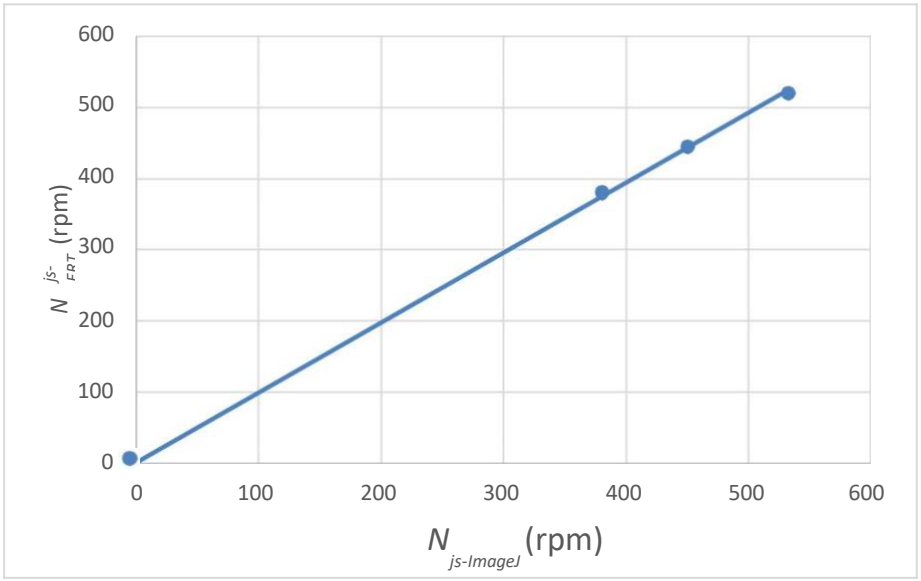

Figure 3.8 $N_{js\text{-}ERT}$ vs $N_{js\text{-}ImageJ}$ Comparison for FBT Impeller with D/T=0.35 and with C/T=0.25, C/T=0.33, C/T= 0.4

3.1.4 Results for DT Impeller

Table 3.5 presents the results obtained with the DT impeller with D/T=0.39 and Figure 3.9 and Figure 3.10 parity plots in of $N_{js\text{-}ERT}$ vs. $N_{js\text{-}Zwietering}$ and $N_{js\text{-}ERT}$ vs. $N_{js\text{-}ImageJ}$, respectively. Similarly, Table 3.6 presents the results obtained with the DT impeller with D/T=0.46 and Figure 3.11 and Figure 3.12 parity plots in of $N_{js\text{-}ERT}$ vs. $N_{js\text{-}Zwietering}$ and $N_{js\text{-}ERT}$ vs. $N_{js\text{-}ImageJ}$, respectively. As one can see, there is significant agreement between the newly proposed ERT method and the other two methods. The typical difference between $N_{js\text{-}ERT}$ and the $N_{js\text{-}Zwietering}$ was 0.86% and that between $N_{js\text{-}ERT}$ and the $N_{js\text{-}ImageJ}$ was 2.00%.

Table 3.5 N_{js} Values Obtained from 3 Different Methods with Using DT Impeller, D/T=0.39, with Different C/T

C/T	$N_{js\text{-}ERT}$ **(rpm)**	$N_{js\text{-}Zwietering}$ **(rpm)**	$N_{js\text{-}ImageJ}$ **(rpm)**
0.25	376	375	373
0.33	378	375	374
0.4	380	380	384

Table 3.6 N_{js} Values Obtained from 3 Different Methods with Using DT Impeller, D/T=0.46, with Different C/T

C/T	$N_{js\text{-}ERT}$ **(rpm)**	$N_{js\text{-}Zwietering}$ **(rpm)**	$N_{js\text{-}ImageJ}$ **(rpm)**
0.33	305	310	317
0.25	284	280	291
0.2	278	275	286

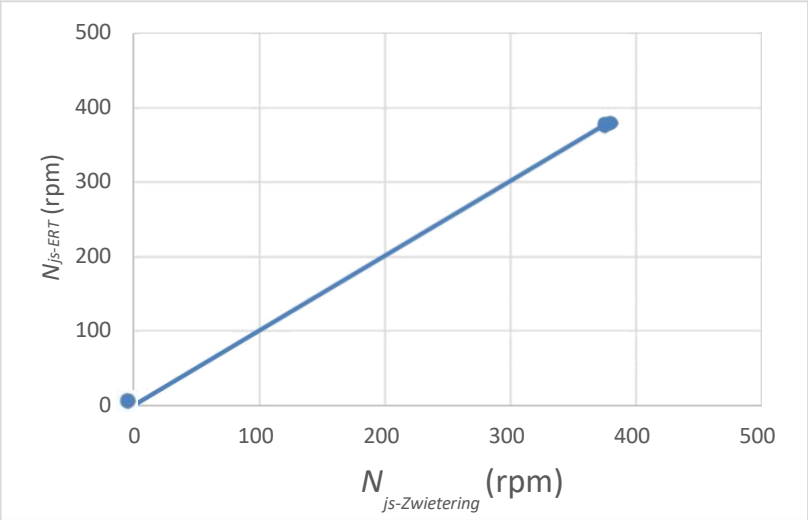

Figure 3.9 $N_{js\text{-}ERT}$ vs $N_{js\text{-}Zwietering}$ Comparison for DT Impeller with D/T=0.39 and with C/T=0.25, C/T=0.33, C/T= 0.4

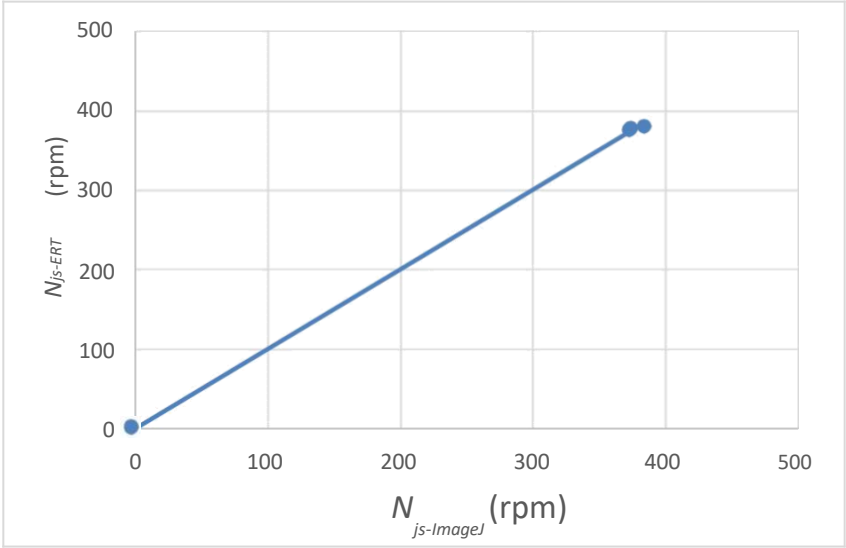

Figure 3.10 $N_{js\text{-}ERT}$ vs $N_{js\text{-}Zwietering}$ Comparison for DT Impeller with D/T=0.39 and with C/T=0.25, C/T=0.33, C/T= 0.4

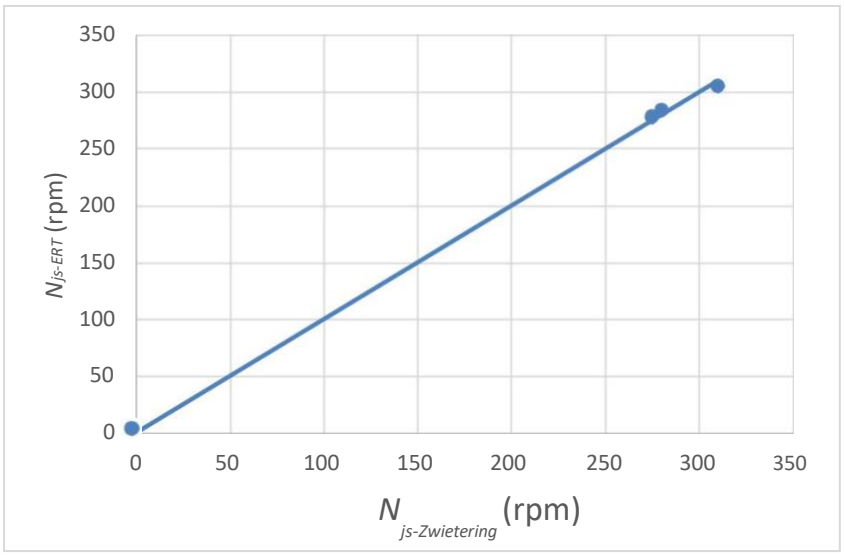

Figure 3.11 $N_{js\text{-}ERT}$ vs $N_{js\text{-}Zwietering}$ Comparison for DT Impeller with D/T=0.46 and with C/T=0.2, C/T=0.25, C/T= 0.33

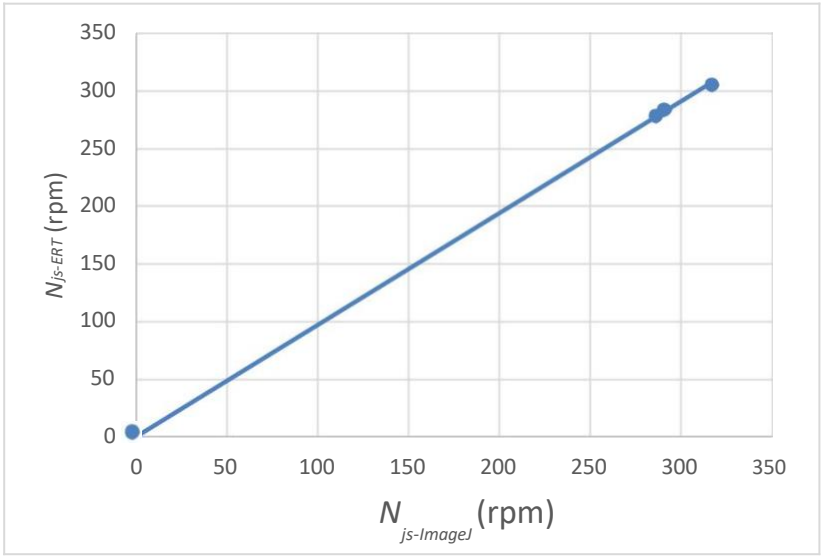

Figure 3.12 $N_{js\text{-}ERT}$ vs $N_{js\text{-}ImageJ}$ Comparison for DT Impeller with D/T=0.46 and with C/T=0.2, C/T=0.25, C/T= 0.33

3.1.5 Results for Propeller

Table 3.7 presents the results obtained with propeller with D/T=0.35 and Figure 3.13 and Figure 3.14 parity plots in of $N_{js\text{-}ERT}$ vs. $N_{js\text{-}Zwietering}$ and $N_{js\text{-}ERT}$ vs. $N_{js\text{-}ImageJ}$, respectively. As one can see, there is significant agreement between the newly proposed ERT method and the other two methods. The typical difference between $N_{js\text{-}ERT}$ and the $N_{js\text{-}Zwietering}$ was 1.42% and that between $N_{js\text{-}ERT}$ and the $N_{js\text{-}ImageJ}$ was 0.47%.

Table 3.7 N_{js} Values Obtained from 3 Different Methods with Using Propeller, D/T=0.35, with Different C/T

C/T	$N_{js\text{-}ERT}$ **(rpm)**	$N_{js\text{-}Zwietering}$ **(rpm)**	$N_{js\text{-}ImageJ}$ **(rpm)**
0.25	528	530	531
0.33	538	545	548
0.5	580	595	591

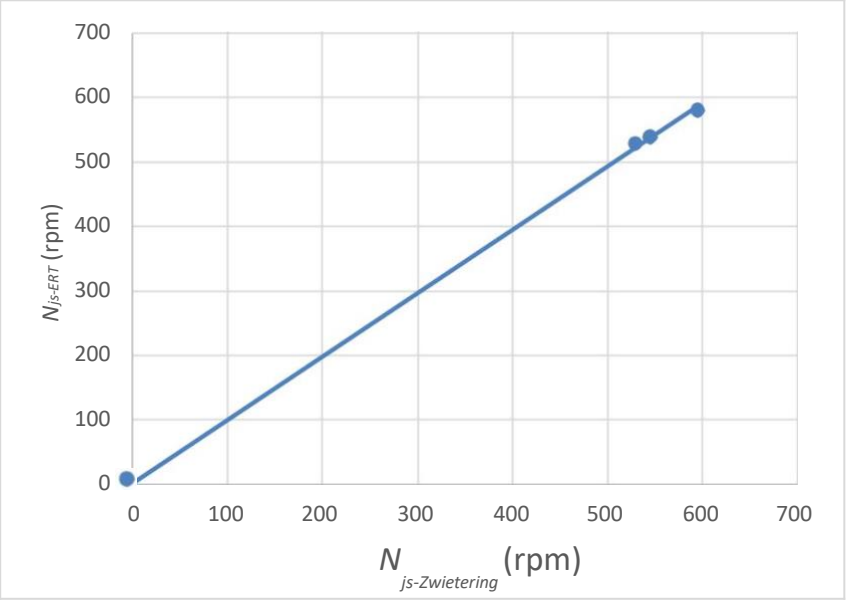

Figure 3.13 $N_{js\text{-}ERT}$ vs $N_{js\text{-}Zwietering}$ Comparison for Propeller with D/T=0.35 and with C/T=0.25, C/T=0.33, C/T= 0.5

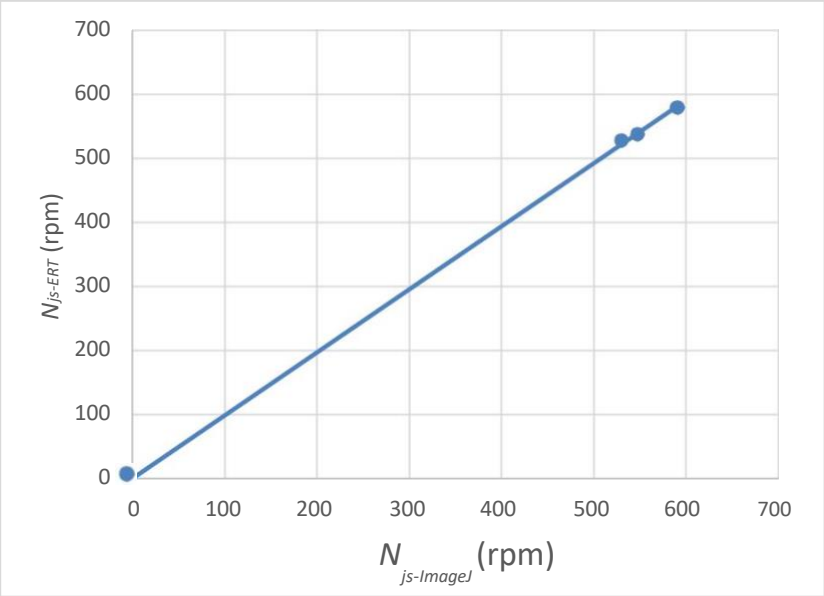

Figure 3.14 $N_{js\text{-}ERT}$ vs $N_{js\text{-}ImageJ}$ Comparison for Propeller with D/T=0.35 and with C/T=0.25, C/T=0.33, C/T= 0.5

For all the impellers, N_{js} increased with increasing impeller height. The reason is, if the impeller gets far away from the bottom, it should have more energy to create a similar flow that can reach the bottom. Furthermore, increasing impeller diameter decreased N_{js}, because bigger impellers create a similar flow more easily and they require less energy.

3.1.6 Cumulative Results

A parity plot showing comparisons of $N_{js\text{-}ERT}$ vs. $N_{js\text{-}Zwietering}$ and $N_{js\text{-}ERT}$ vs. $N_{js\text{-}ImageJ}$, respectively for the all impellers and geometric configurations studied here is presented in Figure 3.15 and Figure 3.16. One can clearly observe that the agreement in both cases was good, indicating that novel method proposed here is appropriate for the determination of N_{js}.

The proposed approach could be especially valuable in all those systems, such as industrial vessels, in which N_{js} would be difficult to obtain with the other methods, which require transparent tanks and the ability to observe the tank bottom.

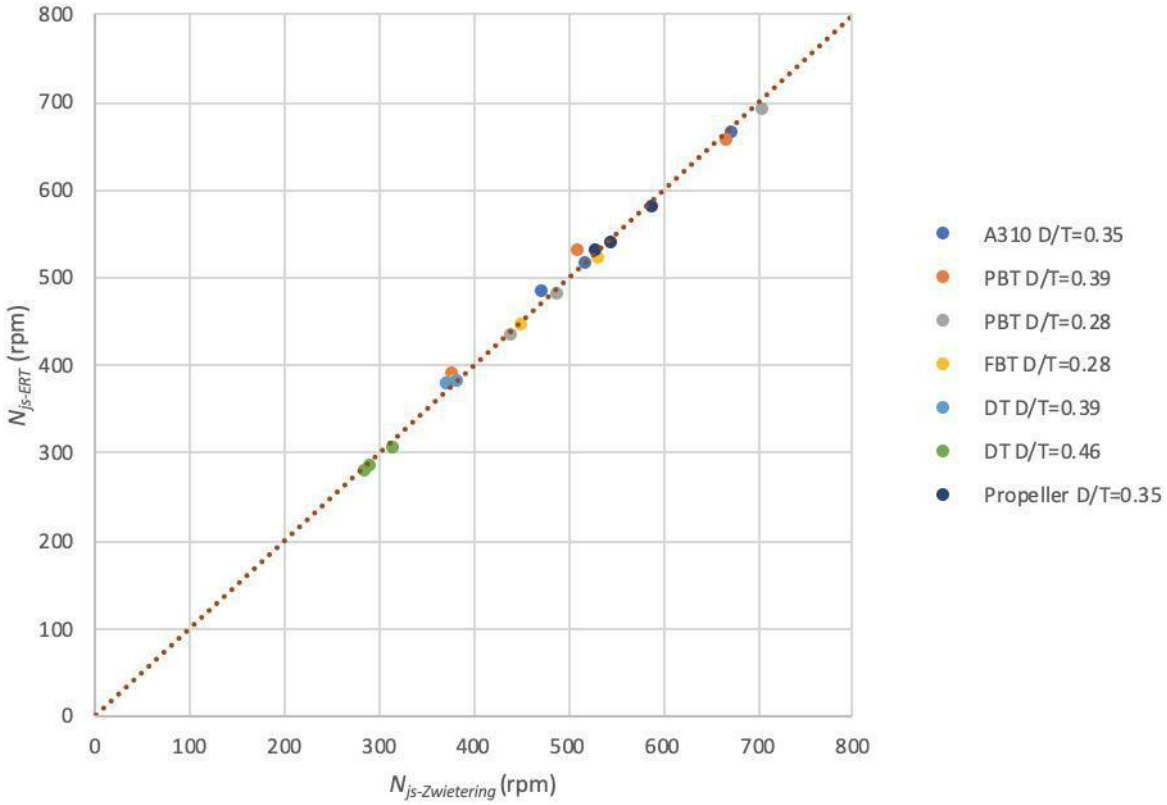

Figure 3.15 $N_{js\text{-}ERT}$ vs $N_{js\text{-}Zwietering}$ Comparison for All The Impellers Used In Different C/T and D/T.

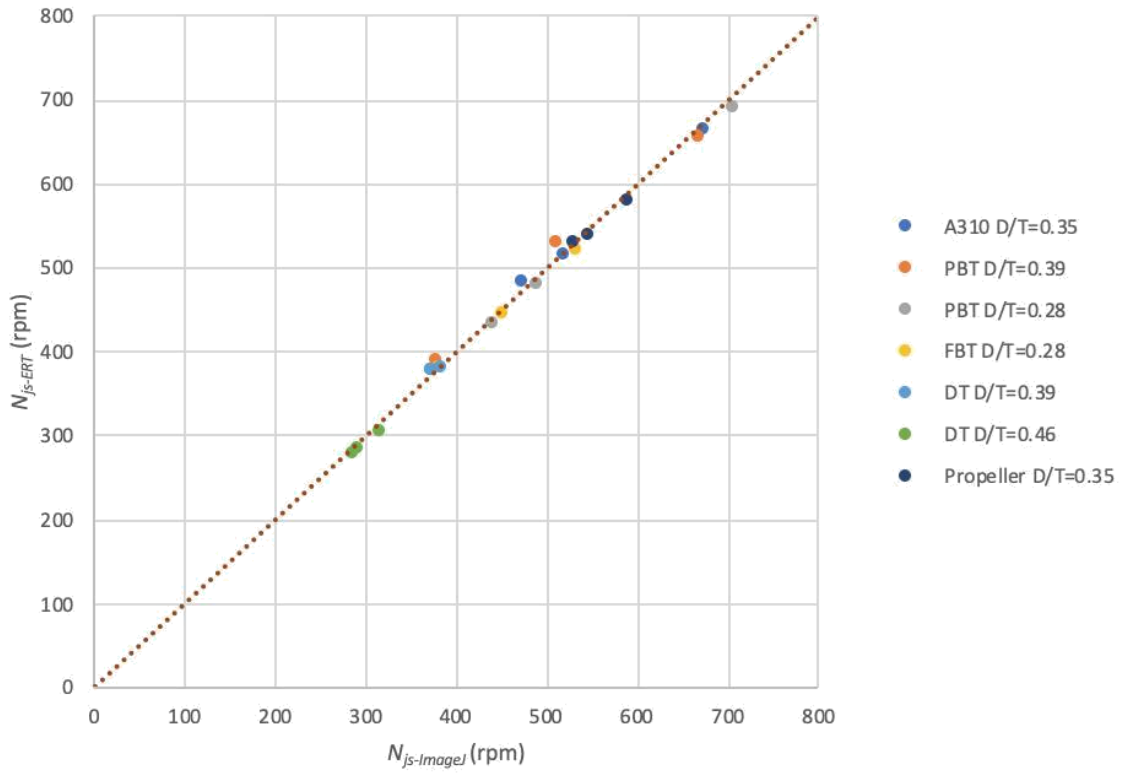

Figure 3.16 $N_{js\text{-}ERT}$ vs $N_{js\text{-}ImageJ}$ Comparison for All The Impellers Used In Different C/T and D/T.

3.2 Reproducibility Analysis

The reproducibility of the N_{js} measurement obtained with the ERC method was found by re-running some experiments 5 times and analyzing the data using an identical approach. The results are presented in Tables 3.8, 3.9 and 3.10 for different impellers. These tables show that the reproducibility was ±2% of the average value in all cases, corresponding to an error of the estimate N_{js} value of about 7 rpm.

3.2.1 Reproducibility Analysis for A310 Impeller with C/T = 0.25

Table 3.8 Reproducibility Analysis for A310 Impeller with C/T = 0.25

Trial #	Njs-ERT
1	484
2	490
3	472
4	478
5	482
Sample Standard Deviation, s	6.723094526
Variance (Sample Standard), s2	45.2
Population Standard Deviation, σ	6.013318551
Variance (Population Standard), σ2	36.16
Sum:	2406
Mean (Average):	481.2
Standard Error of the Mean (SE$\bar{x}$):	3.006659276
Std. Dev/Mean	0.013971518

3.2.2 Reproducibility Analysis for DT Impeller with C/T = 0.2

Table 3.9 Reproducibility Analysis for DT Impeller with C/T = 0.2

Trial #	Njs-ERT
1	284
2	282
3	276
4	278
5	290
Sample Standard Deviation, s	5.477225575
Variance (Sample Standard), s2	30
Population Standard Deviation, σ	4.898979486
Variance (Population Standard), σ2	24
Total Numbers, N	5
Mean (Average):	282
Standard Error of the Mean (SE$\bar{x}$):	2.449489743
Std. Dev/Mean	0.019422786

3.2.3 Reproducibility Analysis for PBT Impeller with C/T = 0.25

Table 3.10 Reproducibility Analysis for PBT Impeller with C/T= 0.25

Trial #	Njs-ERT
1	372
2	388
3	376
4	378
5	388
Total numbers (N):	5
Mean (average) value:	380.4
Population standard deviation (σ):	6.499230724
Population variance (σ2):	42.24
Sample standard deviation (s):	7.26636085
Sample variance (s2):	52.8
Standard Error of the Mean (SE$\bar{x}$):	2.449489743
Std Dev/Mean	0.019101895

CHAPTER 4

CONCLUSION

In this work, the minimum agitation speed, N_{js}, to achieve the just-solid suspension state in stirred tanks was investigated using a novel experimental approach based on the use of Electrical Resistance Tomography (ERT) was investigated. To do so a lab-scale flat bottomed vessel geometrically, similar to those used in pharmaceutical and chemical industries, provided with different types of impellers (six-blade disk turbine, six-blade pitched-blade turbine, A310 turbine, six-blade turbine or propeller) with different D/T, and C/T was used under fully baffled conditions.

By using commercially available ERT device, mean bulk resistivity values R were obtained at increasing higher agitation speeds. Plotting R vs. N resulted in an *S* shaped curve, in which there was a sudden increase in R with increasing agitation speeds before the curve went through an inflexion point and eventually reached an asymptotic value. Lifting solids caused these changes in mean bulk resistivity. Greater resistivity was measured with increasing solids suspension. Once all the solids were lifted up, the mean bulk resistivity did not change anymore.

In order to extract N_{js} from the data, a mathematical approach previously developed by our group for a different system but now applied to the data obtained with the ERT device was used. The reproducibility of replicate experiments showed that the measurement were highly reproductible (within 2%), which proved that the tomography method is a quite reliable method for the determination of N_{js}.

Experiments were conducted where N_{js} was obtained under different operating conditions, i.e., where the impeller type, impeller ratio-to-tank diameter ratio, and impeller clearance were varied. N_{js} was not only experimentally obtained using the proposed ERT approach but also using the Zwietering method as well as the method previously developed by our group. Then, parity plots were constructed in which $N_{js\text{-}ERT}$ was plotted against the N_{js} values obtained with the other two methods. Excellent agreement was observed in all plots, indicating that the novel method proposed here can be effectively used for the experimental determination of N_{js}.

The results of this work show that ERT combined with the analysis of the data proposed here can be used to effectively measure N_{js} in solid-liquid dispersion in mechanically stirred vessels. The proposed approach is observer-independent method and can be used even in systems that cannot be directly observed, such as industrial tanks. Therefore, it is expected that this approach could find extensive practical applications in the chemical, pharmaceutical and biopharmaceutical industries.

APPENDIX

Table A1: Overall N_{js} Results

Clearance	Method	Impeller Type & Diameter						
		DT		PBT		FBT	Propeller	A310
		DT 1	DT 2	PBT 1	PBT 2			
0.2	$N_{js\text{-}Zwietering}$	N/A	275	N/A	430	N/A	N/A	N/A
	$N_{js\text{-}ERT}$	N/A	278	N/A	432	N/A	N/A	N/A
	$N_{js\text{-}ImageJ}$	N/A	286	N/A	440	N/A	N/A	N/A
0.25	$N_{js\text{-}Zwietering}$	375	280	365	475	390	530	470
	$N_{js\text{-}ERT}$	376	284	388	480	380	528	482
	$N_{js\text{-}ImageJ}$	373	291	378	489	381	531	474
0.33	$N_{js\text{-}Zwietering}$	375	310	515	680	460	545	530
	$N_{js\text{-}ERT}$	378	305	530	610	445	538	515
	$N_{js\text{-}ImageJ}$	374	317	512	708	451	548	521
0.4	$N_{js\text{-}Zwietering}$	380	N/A	675	N/A	530	N/A	N/A
	$N_{js\text{-}ERT}$	380	N/A	655	N/A	520	N/A	N/A
	$N_{js\text{-}ImageJ}$	384	N/A	668	N/A	533	N/A	N/A
0.5	$N_{js\text{-}Zwietering}$	N/A	N/A	N/A	N/A	N/A	595	660
	$N_{js\text{-}ERT}$	N/A	N/A	N/A	N/A	N/A	580	665
	$N_{js\text{-}ImageJ}$	N/A	N/A	N/A	N/A	N/A	591	674
Diameters: DT 1 = 11 cm, DT 2 = 13 cm, PBT 1 = 11 cm, PBT 2 = 8 cm, FBT = 10 cm, Propeller = 10 cm, A310 = 10 cm								

APPENDIX

(Continued)

Table A2: Overall Reproducibility Results

Trial #	$N_{js\text{-}ERT}$ (DT) (C/T=0.2)	$N_{js\text{-}ERT}$ (A310) (C/T=0.25)	$N_{js\text{-}ERT}$ (PBT) (C/T=0.25)
1	284	484	372
2	282	490	388
3	276	472	376
4	278	478	378
5	290	482	388
Sample Standard Deviation, s	5.477225575	6.723094526	5
Variance (Sample Standard), s^2	30	45.2	1902
Population Std. Dev., σ	4.898979486	6.013318551	380.4
Variance (Population Standard), σ^2	24	36.16	6.499230724
Total Numbers, N	5	5	42.24
Sum:	1410	2406	7.26636085
Mean (Average):	282	481.2	52.8
Standard Error of the Mean ($SE_{\bar{x}}$):	2.449489743	3.006659276	2.449489743
Std. Dev/Mean	0.019422786	0.013971518	0.019101895

REFERENCES

1. Jafari, R., Tanguy, P.M., Chaouki, J., "Characterization of Minimum Impeller Speed for Suspension of Solids in Liquid at High Solid Concentration, Using Gamma-Ray Densitometry", 2012. *International Journal of Chemical Engineering*, 2012, Article ID 945314.

2. Stanley, S.J., Bolton, G.T., 2008. "A review of recent electrical resistance tomography (ERT) applications for wet particulate processing", *Part. Syst. Charact.*, 25, 207–215.

3. Sharifi, M., Young, B., 2013. "Electrical Resistance Tomography (ERT) applications to Chemical Engineering" *Chemical Engineering Research and Design*, 91, 1625-1645.

4. Mann, R., Dickin, F.J., Wang, M., Dyakowski, T., Williams, R.A., Edwards, R.B., Forrest, A.E., Holden, P.J., 1997a. "Application of electrical resistance tomography to interrogate mixing processes at plant scale", *Chemical Engineering Science*, 52 (13), 2087-2097.

5. Miettinen, T., Laakhonen, M., Aittamaa, J., 2003. "Comparison of various flow visualization techniques in a gas-liquid mixed tank", *Computer Aided Chemical Engineering*, 14, 773-778.

6. Simmons, M.J.H., Edwards, I., Hall, J.F., Fan, X., Parker, D.J., Stitt, E.H., 2009. "Techniques for visualization of cavern boundaries in opaque industrial mixing systems", *AIChe Journal*, 55 (11), 2765-2772.

7. Stanley, S.J., Mann, R., Primrose, K., "Tomographic Imaging of Fluid Mixing in Three Dimensions for Single-Feed Semi-Batch Operation of a Stirred Vessel", 2002. *Chemical Engineering Research and Design*, 80 (8), 903-909.

8. Zwietering, T. N. "Suspending solid particles in liquids by agitators.", 1958. *Chem. Eng. Sci.*, 8, 244-253.

9. Shastry, Shriarjun, "Novel experimental method for the determination of the minimum agitation speed for solids suspension in flat-bottomed stirred tank reactors", 2016. *Theses*. 9.

10. Ricard, F., Brechtelsbauer, C., Xu X.Y., Lawrence C.J., 2005. "Monitoring of multiphase pharmaceutical processes using electrical resistance tomography", *Chemical Engineering Research and Design*, 83(A7): 794–805.

11. Armenante, P.M., Abu-Hakmeh, E.A., 1994. "A Novel Method for the Experimental Determination of the Minimum Agitation Speed for Complete Liquid Dispersion in Agitated Liquid-Liquid-Gas Systems", *Trans IChemE*, 72, Part A.

12. Armenante, P.M., Huang, Y.T., Li, T., 1992. “Determination of The Minimum Agitation Speed to Attain The Just Dispersed State In Solid-Liquid and Liquid-Liquid Reactors Provided With Multiple Impellers”, *Chemical Engineering Science*, 47, No 9-11, 2865-2870.